






## Gate-controlled unitary operation on flying spin qubits in quantum Hall edge states

Takase Shimizu <sup>\*</sup>, Taketomo Nakamura , Yoshiaki Hashimoto, Akira Endo , and Shingo Katsumoto   
*Institute for Solid State Physics, The University of Tokyo, 5-1-5 Kashiwanoha, Kashiwa, Chiba 277-8581, Japan*

 (Received 7 October 2020; revised 30 November 2020; accepted 1 December 2020; published 16 December 2020)

The spin and orbital freedoms of electrons traveling on spin-resolved quantum Hall edge states (quantum Hall ferromagnets) are maximally entangled. The unitary operations on these two freedoms are hence equivalent, which means that one can manipulate the spins with nonmagnetic methods through the orbitals. Taking the quantization axis of the spins along the magnetization axis, the zenith angle is determined by the partition rate of spin-separated edges, while the azimuth angle is defined as the phase difference between the edges. Utilizing these properties, we have realized an electrically controlled unitary operation on the electron spins on quantum Hall ferromagnets. The zenith angle of the spin was controlled through the radius of gyration at a corner by applying voltage to a thin gate placed at one edge. The subsequent rotation in the azimuth angle was controlled via the distance between the edge channels also by a gate voltage. The combination of the two operations constitutes a systematic electric operation on spins in quantum Hall edge channels.

DOI: [10.1103/PhysRevB.102.235302](https://doi.org/10.1103/PhysRevB.102.235302)

### I. INTRODUCTION

Electron spins in semiconductor nanostructures such as quantum dots are expected to serve as qubits for practical quantum computation [1]. The flying qubit (FQ) scheme, which is the usage of traveling electron spins as qubits, is not only indispensable for long-distance entanglement [2,3] between localized arrays of qubits, but is also usable for unitary operations on qubits [4]. The flying spin qubits (FSQs) for electrons considered and tested so far are mostly based on quantum wires with Rashba and Dresselhaus spin-orbit interactions (SOIs) [5–7], which work as a magnetic field effective only on spins [8]. A convenient way to describe unitary transformations on an FQ is obtained by viewing the traveling electron from the coordinate fixed at the center of the electron wave packet (center coordinate). Then, a spatially local Hamiltonian  $H_{\text{loc}}$  can be introduced to describe the dynamics other than translational motion. That is, the travel of a wave packet through a quantum wire with spatial potential modulation can be viewed as a process in which the local Hamiltonian evolves with time [9,10], i.e., the effective Schrödinger equation for the wave packet  $|\Phi\rangle$  at the center coordinate is written as

$$i\hbar \frac{\partial |\Phi\rangle}{\partial t} = H_{\text{loc}}(t) |\Phi\rangle. \quad (1)$$

In this picture, the SOI term in the Hamiltonian also varies with time, which can cause a unitary transformation of the spin freedom in  $|\Phi\rangle$  through a nonadiabatic transition.

Here, we would like to show that there is another type of SOI without a term that explicitly contains  $\hat{p}$  (momentum operator) and  $\hat{s}$  (spin operator) in  $H_{\text{loc}}$ . Generally, an interaction term in a Hamiltonian introduces quantum entanglement [11]

between initially unrelated subsystems. Conversely, when we prepare an initial state with finite quantum entanglement, the interaction appears between subsystems without any interaction term in the Hamiltonian [12], which is well known as the Einstein-Podolsky-Rosen (EPR) paradox [13].

For example, let us consider a wave packet  $|\Phi\rangle$  with Stern-Gerlach-type entanglement [14] between the orbital  $\{|\xi\rangle, |\eta\rangle\}$  and spin  $\{|\uparrow\rangle, |\downarrow\rangle\}$  as

$$|\Phi\rangle = |\xi\rangle \left( \cos \frac{\theta}{2} |\uparrow\rangle \right) + |\eta\rangle \left( e^{i\phi} \sin \frac{\theta}{2} |\downarrow\rangle \right) \quad (0 \leq \phi < 2\pi, 0 \leq \theta \leq \pi), \quad (2)$$

where  $\langle \xi | \xi \rangle = \langle \eta | \eta \rangle = 1$ ,  $\langle \xi | \eta \rangle = 0$ , and  $\phi$  and  $\theta$  are the azimuth and zenith angles of the spin, respectively. We assume that  $H_{\text{loc}}(t)$  has no operator on  $\{|\uparrow\rangle, |\downarrow\rangle\}$ ; thus, there is no explicit interaction term for a certain period, in which the orbital part evolves to  $e^{i\chi}(|\xi\rangle, e^{i\varphi}|\eta\rangle)$ . Here,  $\chi$  is the phase developed as the wave packet travels, while  $\varphi$ , the phase difference resulting from the path difference, etc., can be absorbed into the azimuth angle of the spin. The process hence can be viewed as translational motion with spin precession, which is simply a phenomenon associated with an effective magnetic field by an SOI [15]. The equivalence of the phenomena with a quite different appearance reflects the inseparability of systems with maximal entanglement. This idea also suggests the possibility of manipulating the electron spins through orbital motion, the architecture for which is theoretically proposed in Ref. [16].

The quantum coherence length of the one-dimensional channel for FQ propagation should be long enough to preserve quantum information. In solids, the longest coherence lengths have been reported for quantum Hall edge channels (QHECs) [17,18], which are thus strong candidates for FQ channels. QHECs are known to show spin separation at comparatively low magnetic fields with the aid of an exchange interaction

\*takase@issp.u-tokyo.ac.jp

[19], transforming into ferromagnetic phases [20,21]. In such a ferromagnetic regime, the entanglement of spin and edge channels occurs, naturally preparing for the realization of the scheme in (2). A preliminary experiment on such precession control was reported by Nakajima *et al.* [22,23]. For zenith angle tuning, a controlled splitting of the wave packet into two channels is required. Such experiments have been reported by Deviatov *et al.* [24–26] with the use of current imbalance, and by Karmakar *et al.* [27,28] with the use of periodic magnetic gates.

In this paper, we present experimental results regarding the unitary operations of FSQ in spin-polarized QHECs in the above scheme with electrostatic gates. With respect to Eq. (2), a rotation in the zenith angle corresponds to tunneling between spin-polarized QHECs. It is shown that this can be achieved by the sharp bending of the edge line. At such a corner, an angular momentum in the edge orbital emerges, and Landau-Zener-type tunneling brings about a rotation in the zenith angle. The rate of Landau-Zener tunneling depends on the sharpness of the corner. With the addition of a thin gate to vary the sharpness, we show that the zenith angle can be controlled more simply. We should note that the same physics can be described in the terms for the quantum Hall effects. We believe the present description will bring a fresh perspective to the traditional quantum Hall effects.

## II. EXPERIMENTAL METHOD

Figures 1(a)–1(c) describe the experimental setup in three different ways for a two-dimensional electron system (2DES) in the spin-split quantum Hall regime. For simplicity, the filling factor  $\nu$  is chosen to be 2 in the figure, although the region of  $\nu = 4$  was mostly used in the present experiment. Figure 1(a) is a schematic of wave-propagation paths, Fig. 1(b) shows the gate-electrode configuration for realizing them, and Fig. 1(c) illustrates a blowup of the down edges of the side gates (SL, SR) and center gate (C) along with the propagation paths in Fig. 1(a). The sample edges have two QHECs for  $\nu = 2$ , which we here denote channel 1 and channel 2, in which spins are locked at  $\uparrow$  and  $\downarrow$ , respectively. Then, we can write their wave packet as  $|1\rangle|\uparrow\rangle$  and  $|2\rangle|\downarrow\rangle$ , respectively, where  $|1\rangle$  and  $|2\rangle$  are the normalized wave functions of the orbital part.

Let us trace a wave packet that is emitted from the right electrode. Beneath the gates L and R, the filling factors  $\nu_L$  and  $\nu_R$  are tuned to 1, and only channel 1 goes through them [29,30]. Hence, the incident wave packet in Fig. 1(a) can be written as  $|\psi_1\rangle|\uparrow\rangle$ . Channels 1 and 2 meet at the lower right corner edge of the gate SR, where a partial transfer occurs through a local SOI as a result of the orbits wrapping around the sharp corner. This scattering process is written as

$$|1\rangle|\uparrow\rangle \rightarrow |\Phi\rangle_{\text{SR}} = t_{11R}|1\rangle|\uparrow\rangle + t_{12R}|2\rangle|\downarrow\rangle, \quad (3)$$

where  $t_{ijR}$  are the complex transmission coefficients of the processes  $|i\rangle \rightarrow |j\rangle$  at the right corner satisfying the unitary condition  $|t_{11R}|^2 + |t_{12R}|^2 = 1$  because of the perfect chirality of the QHEC. Hence, they can be written as  $t_{11R} = \cos\theta/2$  and  $t_{12R} = e^{i\phi_0}\sin\theta/2$ , where  $\theta$  reflects the amplitude ratio of the partial waves and  $\phi_0$  is the phase difference between  $t_{11R}$  and  $t_{12R}$ . Thus,  $|\Phi\rangle_{\text{SR}}$  is prepared in the form of  $|\Phi\rangle$  in (2).

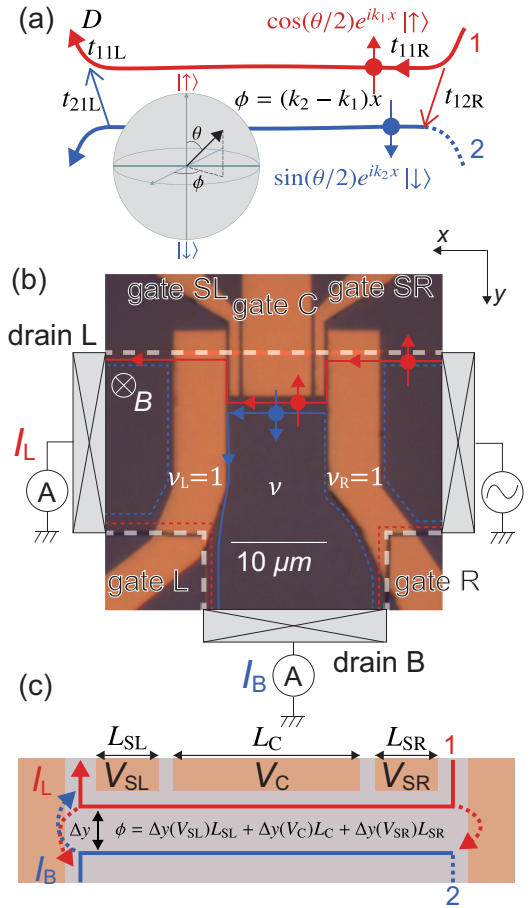


FIG. 1. (a) Schematic diagram of the “quantum circuit” for electron wave packets (red and blue circles with arrows indicating spin), with an illustration of the Bloch sphere description of an FSQ. (b) Optical micrograph of the sample with an external circuit illustration. The orange regions are metallic gates, three of which are annotated. The 2DES substrate is trimmed at the white dashed lines. (c) illustrates the hybridization of (a) and (b) around the lower ends of the gate SL, C, and SR.

In QHEC, the orbital part of the wave function in the single-electron picture is written as a quasi-one-dimensional plane wave in a real-space representation [31],

$$\psi_i(\mathbf{r}) \propto \exp(ik_i x) \exp\left[-\frac{(y - y_i)^2}{2l^2}\right], \quad (4a)$$

$$y_i = -l^2 k_i, \quad (4b)$$

where  $l$  ( $=\sqrt{\hbar/eB}$ ,  $B$  is the magnetic field) is the magnetic length,  $i$  is the channel index counted from outer (lower energy in bulk) to inner, the  $x$ -axis direction is taken as along the one-dimensional channel, and  $y_i$  is the guiding center position. In the edge states,  $\psi_i$  accommodates the propagating wave packet  $|i\rangle$ .  $|i\rangle$  travels on  $\psi_i$  along the down edges of the gate SR, C, and SL, thereby gaining a kinetic phase. At the end of the travel over total length  $L$ , the difference in the acquired kinetic phase or the azimuth angle rotation of the spin is

$$\phi = (k_1 - k_2)L \quad (5a)$$

$$= \frac{(y_2 - y_1)L}{l^2} = 2\pi \frac{\Delta y LB}{h/e}. \quad (5b)$$

Because  $\Delta y LB/(h/e)$  is the magnetic flux piercing the area between the two paths measured in units of flux quantum ( $h/e$ ), the difference in kinetic phase acquired in the travel over the two channels is equal to the Aharonov-Bohm (AB) phase caused by the magnetic field. Thus, we can tune  $\phi$  using both the magnetic field and the voltage supplied to gate C, which varies the interval  $\Delta y$  between the edge states. This single-electron picture requires a correction with consideration of the screening effect, as will be discussed in the analysis sections, although the above results can still be applied to real experiments with some modifications, e.g.,  $B$  dependence of  $\Delta y$  as given in Eq. (7).

At the left corner of the gate SL, channel 1 with  $\uparrow$  goes up to go beneath the region of  $\nu_L = 1$ , while channel 2 with  $\downarrow$  goes down to turn around the region. Because both channels change their directions abruptly, a crossing transition between them by a local SOI occurs at the corner, as illustrated in Figs. 1(a) and 1(c). In this two-in-two-out vertex, the partition ratio is affected by the phase  $\phi - \phi_0$ , and the traverse across the sample ends up at drain L or drain B with the probabilities determined by the ratio. Hence, the partition ratio can be measured as the ratio of the current through L ( $I_L$ ) to the total current ( $I_L + I_R$ ), i.e., current distribution ratio  $D \equiv I_L/(I_L + I_R)$ . In a simple model of the two-in-two-out vertex described in Sec. IV,  $D$  is written as

$$D = C_0 + C_1 \sin \theta \cos(\phi + \Delta\phi), \quad (6)$$

where  $\Delta\phi$  represents the phase shift associated with the interedge scattering at the two corners, including  $-\phi_0$ . Equation (6) is similar to the simplest Young's double-slit approximation of an AB interferometer because of the chirality or broken time-reversal symmetry of the channels and multiterminal configuration [32]. The partition ratio of the input affects the visibility, giving the  $\theta$  dependence.

A two-dimensional electron system (2DES) with an electron density of  $4.4 \times 10^{11} \text{ cm}^{-2}$  and a mobility of  $86 \text{ m}^2/\text{V s}$  in an  $\text{Al}_x\text{Ga}_{1-x}\text{As}/\text{GaAs}$  ( $x = 0.265$ ) single heterostructure was used as the base system for the sample. The structure of the wafer was (from the front surface) 5-nm Si-doped GaAs cap layer, 40-nm Si-doped ( $N_{\text{Si}} = 2 \times 10^{18} \text{ cm}^{-3}$ )  $\text{Al}_x\text{Ga}_{1-x}\text{As}$  layer, 15-nm undoped  $\text{Al}_x\text{Ga}_{1-x}\text{As}$  spacer layer, and an 800-nm GaAs layer with a 2DES residing near the interface with the upper layer. The terminal and Au/Ti gate configurations are shown in Fig. 1(b). We cooled the sample down to 20 mK and applied a perpendicular magnetic field  $B$  up to 9 T, at which the 2DES is in the quantum Hall state with a filling factor of  $\nu = 2$ .

An AC voltage of typically  $33 \mu\text{V}_{\text{rms}}$  (except for the measurements in Fig. 5) at 170 Hz was applied to the right-side contact, and the current was measured at drain L and drain B with an  $I$ - $V$  amplifier by standard lock-in measurements. A representative difference of the contact and cable resistance between drains L and B was less than approximately 2%. Therefore,  $D$  is nearly equal to the transmission probability from source to drain L.

The voltage on gate C ( $V_C$ ) modifies the potential gradient in the  $y$  direction along gate C and thus the distance between neighboring edge states  $\Delta y$ , which leads to the modulation of  $\phi$  [22,23].

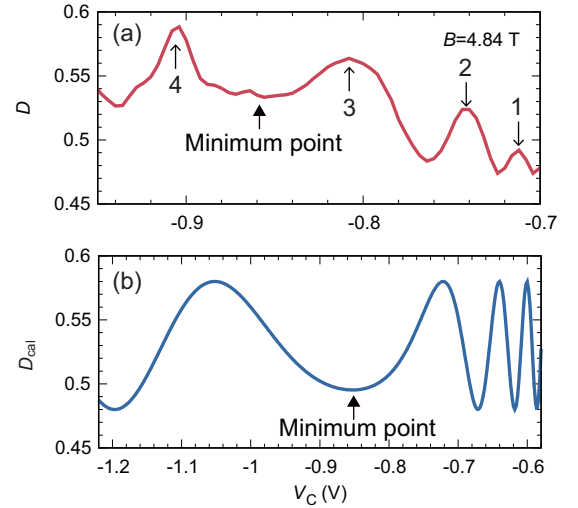


FIG. 2. (a)  $V_C$  dependence of the current distribution ratio  $D$  at  $B = 4.84 \text{ T}$ . Side gate voltages were set to  $V_{\text{SR}} = V_{\text{SL}} = -0.6 \text{ V}$ , where the 2DES under the gates was completely depleted. (b) Calculation example of  $D$  as a function of  $V_C$  based on the model of Eq. (7).  $d = 66 \text{ nm}$  from the one-dimensional Poisson-Schrödinger calculation on the layered structure of the sample (see the Supplemental Material [33]). Other parameters are as follows:  $g = -0.6$  [19];  $\epsilon = 12.35$  [34];  $C_1 \sin(\theta) = 0.05$ ,  $C_0 = 0.53$ ,  $\Delta\phi = 0$ ,  $L_C = 7.5 \mu\text{m}$ ;  $L_{\text{SL}} = L_{\text{SR}} = 1.25 \mu\text{m}$ ; the offset in the gate voltage  $V_C$ ,  $V_{\text{SL}}$ , and  $V_{\text{SR}}$  resulting from the contact built-in potential is  $V_{\text{offset}} = -0.05 \text{ V}$ . See the text for  $n(y)$ .

### III. ROTATION IN AZIMUTH ANGLE

Figure 2(a) shows the  $V_C$  dependence of  $D$  measured at  $B = 4.75 \text{ T}$ , which corresponds to  $\nu = 4$  in the nongated region. The filling factors underneath gate L and gate R were kept at 1 (pinch-off conductance traces for gate L are in the Supplemental Material Sec. III [33]). In this situation, there are two extra edge states inside the 2DEG compared with that illustrated in Fig. 1. In the following experiments, we believe the tunneling rate from the edge states 1 and 2 to these extra states is small and they are negligible at the precision level of the present research; then, the channel indices  $i = 1$  and 2 are under our consideration. The detailed discussion is given in Sec. VII of the Supplemental Material [33]. Side gate voltages were set to  $V_{\text{SR}} = V_{\text{SL}} = -0.6 \text{ V}$ , where the 2DES under the gates was completely depleted. The measured  $D$  shows an oscillation against  $V_C$  in the range from  $-0.7$  to  $-0.98 \text{ V}$ , where four peaks are observable, as indicated by arrows. The oscillation period increased with negative  $V_C$ . The region between peaks 3 and 4 is especially wide, and the line shape shows the rewinding of oscillation. We tested several other samples with essentially the same gate configuration, and such behavior was commonly observed.

To verify the above phase modulation scenario (or equivalent rotation in  $\phi$ ), we need to know how  $\Delta y$  in Eq. (5b) depends on  $V_C$  taking the electric screening effect into account. In the single-electron picture of Eq. (4), the one-dimensional channels are formed on the lines where the Landau levels cross the Fermi level. In more practical treatments in Refs. [35,36], the QHECs are described as

“compressible” stripes separated by “incompressible” insulating regions. In the compressible stripes, the electrostatic potential is kept constant by the screening effect, while the group velocity  $\partial E_i/\hbar\partial k_i$  is finite. Therefore, Eq. (4b) does not hold inside the stripes and the wave number  $k_i$  should also be kept constant. In other words, Eq. (4b) only holds inside the incompressible regions. As the value of  $\Delta y$ , we should thus take the width of the incompressible stripes, which is generally much narrower than that of the compressible ones. In Refs. [35,36], such  $\Delta y$  is explicitly given for a simple classical electrostatic model of the QHEC as

$$\Delta y \approx \sqrt{\frac{8|\Delta E|\epsilon\epsilon_0}{\pi e^2(dn/dy)|_{y=y'_i}}}, \quad (7)$$

where  $y'_i$  is the position of the  $i$ th incompressible liquid strip,  $\epsilon\epsilon_0$  is the dielectric permittivity of the matrix semiconductor,  $n(y)$  is the electron sheet density profile, and  $\Delta E$  is the energy difference between the levels of channels  $i$  and  $i+1$ . The model has been used in analyzing many experimental works [37–39].  $\Delta E$  in the present case ( $i=1$ ) of exchange-aided Zeeman splitting can be written as  $g\mu_B B$ , where  $g$  is the effective Landé  $g$ -factor, and  $\mu_B$  is the Bohr magneton.

Figure 2(b) shows an example of the  $V_C$  dependence of  $D$ , calculated from Eq. (7) with the parameters noted in the caption. These parameters are chosen to preserve semi-quantitative consistency with the analysis of the magnetic response described later. To calculate  $n(y)$  as a function of  $V_C$ , we employ the “frozen surface” model and the self-consistent Thomas-Fermi approximation given in Ref. [36]. Then,  $(dn/dy)|_{y=y'_i}$  can be obtained numerically from  $n(y)$ . The characteristic behavior of the oscillation in Fig. 2(a) is qualitatively reproduced, in that the oscillation phase advances more rapidly with negative  $V_C$  at lower  $|V_C|$ . The progress in the phase slows down, and the rewinding of the oscillation with increasing  $|V_C|$  begins at the point indicated in the figure as the “minimum point.” This behavior is qualitatively explained as follows (a schematic of this description is in the Supplemental Material [33]). At low  $V_C$ , the edge of the 2DES lies near the end of the center gate, and the electrostatic confinement potential at the edge is soft, leading to small  $(dn/dy)|_{y=y'_i}$  and large  $\Delta y$ . With increasing negative  $V_C$ , the potential becomes steeper, lowering  $\Delta y$ . A further increase in negative  $V_C$  causes softening of the potential and an increase in  $\Delta y$  again. Because  $\Delta y$  must be smooth as a function of  $V_C$ ,  $|d(\Delta y)/dV_C|$  decreases with negative  $V_C$ , i.e., the oscillation period becomes slower, until reaching the minimum point, roughly corresponding to the steepest edge confinement potential [maximum in  $(dn/dy)|_{y=y'_i}$ ], and again increases with negative  $V_C$ , resulting in the rewinding of the oscillation in  $D$ .

In spite of the obvious resemblance between Figs. 2(a) and (b), quantitative fitting that is consistent with a response to the magnetic field is difficult. We also investigated the “Fermi-level pinning” model for the surface states, although it did not improve the quantitative agreement. This discrepancy indicates the necessity to take into account the effects not considered, e.g., the geometrical effect of the gate electrode. However, the close resemblance between Figs. 2(a) and 2(b)

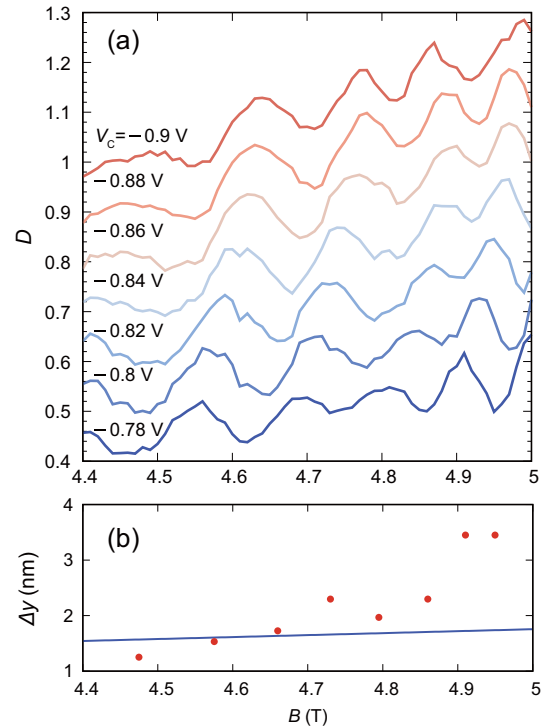


FIG. 3. (a) Current partition rate  $D$  as a function of  $B$  within the plateau regime encompassing the filling factor  $\nu = 4$  for several values of gate C voltage  $V_C$  (traces are offset for clarity).  $V_{ac} = 32.8 \mu V_{rms}$ . (b)  $\Delta y$  calculated from the equation  $\Delta y = (2/3)(h/e)/L\Delta B$  for  $V_C = -0.86$  V.  $\Delta B$  is given by twice the distance between the adjacent oscillation peak and dip. The blue line indicates  $\Delta y_{average} = [\Delta y(V_{SL})L_{SL} + \Delta y(V_C)L_C + \Delta y(V_{SR})L_{SR}]/(L_{SL} + L_C + L_{SR})$  from Eq. (7) with the parameters used in Fig. 2(b).

still manifests the essential correctness of the scenario described so far.

As in Eq. (5b), the azimuth angle rotation is locked to the AB phase acquired from the magnetic flux piercing the incompressible regions. This can be readily confirmed by the oscillatory behavior of  $D$  vs  $B$ , as shown in Fig. 3(a) with  $V_C$  as a parameter. Because a single period  $\Delta B$  of the oscillation corresponds to  $2\pi$  rotation in  $\phi$ ,  $\Delta y$  is given as  $\Delta y = (2/3)(h/e)/L\Delta B$  from Eq. (5b) in the local linear approximation of the  $B$  dependence of  $\Delta y$  in (7), where  $\Delta E = g\mu_B B$  (details of this calculation are described in the Supplemental Material [33]). This gives  $\Delta y$  as a function of  $B$ , as shown in Fig. 3(b) for  $V_C = -0.86$  V. The obtained values of  $\Delta y$  (1–3 nm) are much shorter than the magnetic length  $l = 11$  nm at  $B = 5$  T, which is consistent with the view of compressible/incompressible stripes, while the predicted  $B$  dependence of  $\Delta y$  for constant  $g$  against  $B$  deviates from the experiment, as indicated by Fig. 3(b).

To visualize the overall trend, the measured and calculated values of  $D$  are color plotted on  $B$ - $V_C$  in Figs. 4(a) and 4(b), respectively. The oscillation patterns appear as curved stripes in these plots. Such curving behavior is consistent with the interpretation of Fig. 2 as follows. With an increase in negative  $V_C$  from  $-0.7$  V to approximately  $-0.8$  V for a fixed  $B$ ,  $(dn/dy)|_{y=y'_i}$  increases and  $\phi$  thus decreases,

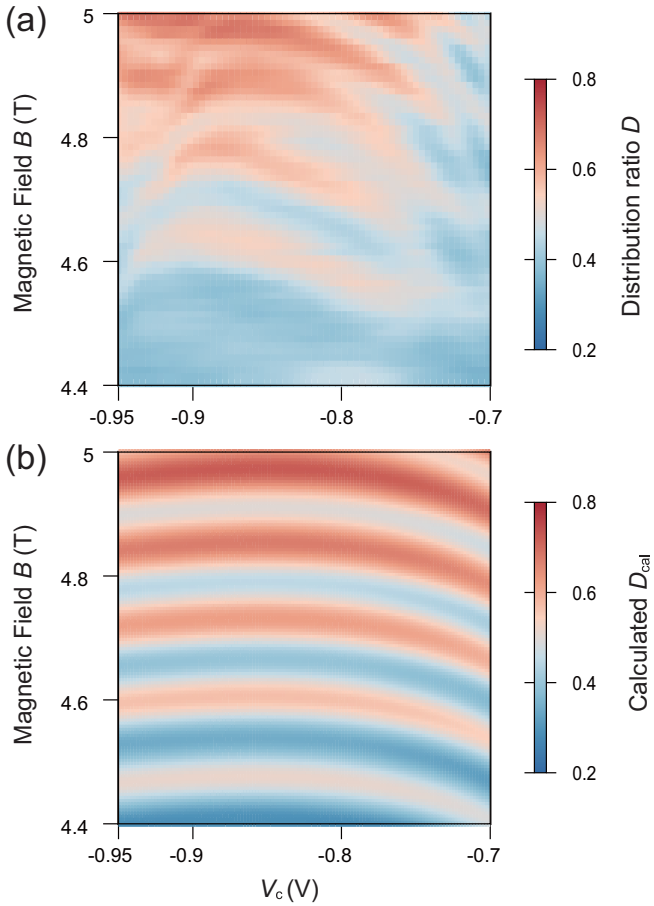


FIG. 4. (a) Color plot of the measured  $D$  as a function of  $B$  and  $V_C$ .  $V_{SR} = V_{SL} = -0.6$  V. (b) Color plot of the theoretically given  $D$  as a function of  $B$  and  $V_C$ .  $C_0 = 0.42B - 1.45$  and  $C_1 \sin(\theta) = 0.1$  are used. The other parameters are the same as those in Fig. 2(b).

corresponding to the up-going ridges. After reaching the maximum at  $V_C \approx -0.86$  V,  $(dn/dy)|_{y=y'_1}$  declines with a further increase in negative  $V_C$ .

The observation of arclike curving strongly supports the legitimacy of the analysis so far. Similar arclike curves were also observed at filling factors  $\nu = 2$  and 3, but with smaller visibility. At smaller filling factors,  $B$  and hence  $\Delta y$  are larger, making  $\theta$ , the zenith angle, smaller, as discussed later. Regarding visibility, in Fig. 2, the oscillation under the present consideration is visible in the range of  $V_C$  from  $-0.7$  to  $-1$  V, and the visibility is highest around the minimum point. This tendency is common in the region  $B$  in Fig. 4, and the visibility does not change very much with  $B$ . Because an increase in  $B$  denotes an enhancement in the rotation of  $\phi$ , the possibility of dephasing by the number of  $\phi$  rotations is eliminated. Instead, we speculate that the simple model in Fig. 1(c) is approximately realized only around the steepest edge potential condition. When the edge potential is soft, the QHECs have more chances to experience the effect of local potential disorder. As a result, the effective edge line fluctuates spatially, creating local orbital angular momentum, which causes interedge state scattering [40]. The above discussion is a possible explanation of the dephasing in  $\phi$  rotation.

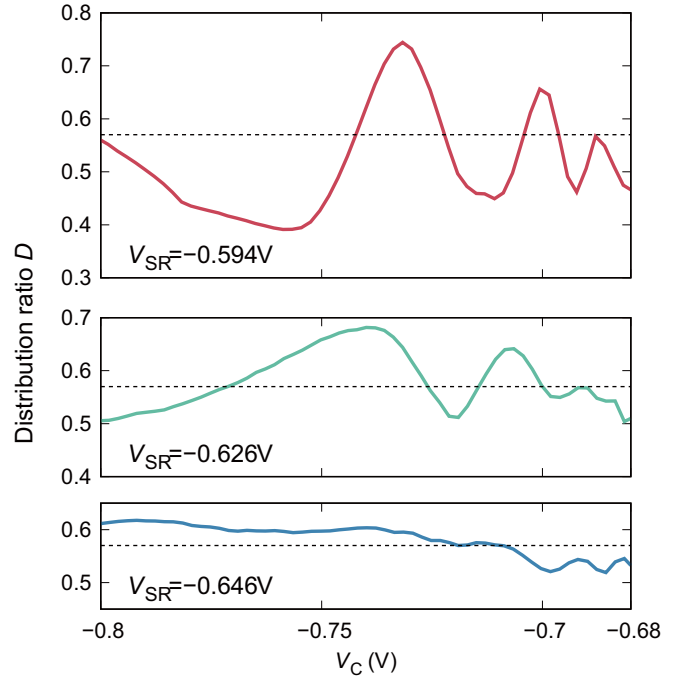


FIG. 5. Three oscillation patterns corresponding to three different values of  $V_{SR}$ .  $B = 4.5$  T and  $V_{SL} = -0.605$  V.  $V_{ac} = 23.8 \mu V_{rms}$ . The line for  $D = 0.57$  is indicated by dashed lines to show that there is almost no movement in the oscillation baseline.

From the above results and analysis, we can safely say that the current partition ratio  $D$  reflects the azimuth angle rotation of FSQ traveling along the down edges of the gates. The rotation angle can be tuned via center gate voltage electrostatically.

#### IV. ROTATION IN ZENITH ANGLE

In Fig. 5, we compare the oscillation patterns for three representative values of  $V_{SR}$ , which strongly affects the oscillation amplitude. From  $V_{SR} = -0.594$  V the amplitude gradually decreases with a further increase in negative  $V_{SR}$ . The characteristic features of the oscillation versus  $V_C$  observed so far do not change with  $V_{SR}$ , other than a phase shift, which is probably caused by a change in  $\phi_0$ . In the region  $V_{SR} > -0.594$  V, the oscillation pattern changed drastically with a slight difference in  $V_{SR}$ . This is probably because channel 2 penetrates the spatial gap between gate C and gate SR. Hence, this region is excluded from the present discussion.

We should thus look for the origin of the amplitude modulation in the zenith angle  $\theta$ , which is determined when the wave packet turns the down-right corner of the gate SR. At the turning point, the time-dependent local Hamiltonian in (1) for the wave packet should contain SOI terms: one from the in-plane potential gradient [41], the other from the Rashba and Dresselhaus effects commonly observed in 2DES [8]. In the present case of spin-polarized QHEC, the former affects the effective Zeeman energy by the spin-orbit effective field, while the latter kinematically rotates the spin. Figure 6(a) illustrates the time evolution of quasideigenenergies for spin-down and spin-up, i.e.,  $E_{\uparrow} = \langle \uparrow | \langle 1 | H_{loc}(t) | 1 \rangle | \uparrow \rangle$  and  $E_{\downarrow} =$

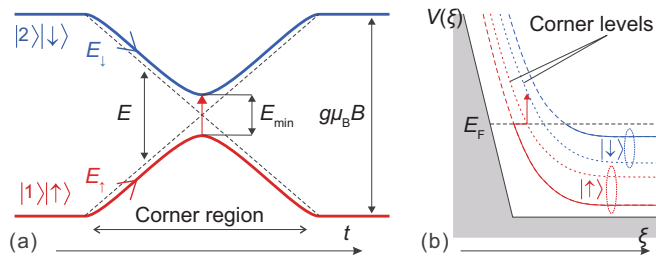


FIG. 6. (a) Schematic time evolution of quasideigenenergies  $E_{\uparrow} = \langle \uparrow | \langle 1 | H_{\text{loc}}(t) | 1 \rangle | \uparrow \rangle$  and  $E_{\downarrow} = \langle \downarrow | \langle 2 | H_{\text{loc}}(t) | 2 \rangle | \downarrow \rangle$ . (b) Illustration of spin-polarized edge states for a straight edge (solid and dashed lines) and a corner (dotted lines).  $\xi$  represents the distance from an edge of infinite potential [ $V(0) = \infty$ ]. For simplicity, the Landau levels are drawn in the single-electron picture.

$\langle \downarrow | \langle 2 | H_{\text{loc}}(t) | 2 \rangle | \downarrow \rangle$ . Around the center of the corner region,  $E = E_{\downarrow} - E_{\uparrow}$  takes the minimum value  $E_{\text{min}}$ .

The transition in Eq. (3) can then be taken as partially nonadiabatic tunneling. By summarizing these effective time-localized SOIs as  $H_{\text{SOI}}(t)$ , the probability  $P$  of the inter-edge channel transition is given by slightly modifying a Landau-Zener-type formula [42] as

$$P \propto |\langle \uparrow | \langle 1 | H_{\text{SOI}} | 2 \rangle | \downarrow \rangle|^2 \exp \left[ -2\pi \frac{(E_{\text{min}}/2)^2}{\hbar(dE/dt)} \right], \quad (8)$$

where  $dE/dt$  is the slew rate of  $E$ . As indicated by the arrows in Fig. 6(b), the total process from  $|1\rangle|\uparrow\rangle$  to  $|2\rangle|\downarrow\rangle$  consists of a nonadiabatic transition from  $|1\rangle|\uparrow\rangle$  to  $|1\rangle|\downarrow\rangle$  and an adiabatic transition from  $|1\rangle|\downarrow\rangle$  to  $|2\rangle|\downarrow\rangle$ . The expression in (8) indicates that the slew rate and the minimum energy difference strongly affect the transition probability.

A simple explanation of the tendency in Fig. 5 follows from Eq. (8) and the electrostatic model in Refs. [35,36]. With increasing negative  $V_{\text{SR}}$ , QHECs move away from the “steepest potential” point, where the distance between the outer and the inner edges is the minimum and the radius of gyration  $r_l$  also is the shortest. As  $r_l$  decreases,  $dE/dt$  increases because of the shorter interaction time, and the potential gradient is larger; thus,  $E_{\text{min}}$  is smaller. From Eq. (8), the transition probability  $P$  is the maximum for the steepest edge potential condition. As in Fig. 5, this scenario tells us that the steepest potential condition should correspond to  $V_{\text{SR}} > -0.594$  V, which is considerably smaller than  $-0.8$  V for  $V_C$ . This difference may come from the geometrical complexity in the real gate configuration. As in the Supplemental Material [33], the equipotential lines around the corner change intricately, and the maximum of  $P$  may appear at smaller  $V_{\text{SR}}$  than the value at the steepest potential.

From the oscillation data in Fig. 5, we can estimate the zenith angle  $\theta$ , assuming that the dephasing is ignorable at the largest amplitude region in  $V_C$  as follows. Even if such ignorable dephasing is not the case, the lower limit of  $\theta$  can be obtained from the analysis. Let  $t_{iL}$  be the complex trans-

mission coefficients of the processes  $|i\rangle \rightarrow |j\rangle$  at the bottom left corner of the gate SL; then, from Eq. (3), the wave-packet state that turns the corner and enters channel 1 to go to drain L is written as

$$|\Phi\rangle_L = (t_{11R}e^{ik_1L}t_{11L} + t_{12R}e^{ik_2L}t_{21L})|1\rangle|\uparrow\rangle.$$

For simplicity of expression, we write the complex transmission coefficients in the modulus-argument form as  $t_{11R}t_{11L} = t_1 \cos(\theta/2)e^{i\varphi_1}$  and  $t_{12R}t_{21L} = t_2 \sin(\theta/2)e^{i\varphi_2}$ . This leads to the simple Young’s double-slit result of the transmission coefficient  $T_L = \langle \Phi | \Phi \rangle_L$  as

$$T_L = t_1^2 \cos^2(\theta/2) + t_2^2 \sin^2(\theta/2) + t_1 t_2 \sin \theta \cos(\phi + \Delta\varphi). \quad (9)$$

From the comparison with Eq. (6),

$$C_0 = t_1^2 + (t_2^2 - t_1^2) \sin^2(\theta/2), \quad C_1 = t_1 t_2. \quad (10)$$

In Fig. 5, the baseline of oscillation  $C_0$  shows almost no change, while  $C_1 \sin \theta$  varies widely. This fact is based on Eq. (10), where  $t_1$  and  $t_2$  happen to be close to each other:  $t_1 \approx t_2$ , in the present condition (the best visibility condition). Then,  $C_0 \approx t_1^2 \approx C_1 \approx 0.57$ . In Fig. 5, the largest amplitude gives  $C_1 \sin \theta$  as 0.17, which corresponds to  $\theta \approx 17.4^\circ$ . This is the lower bound of the estimated  $\theta$ , which inevitably contains an underestimation because of dephasing. To obtain a precise estimation of  $\theta$ , the oscillation of  $C_1 \sin \theta$  should be observed. Unfortunately, in the present case, the maximum obtained value of  $\theta$  is less than  $90^\circ$ , and further analysis is difficult. For more precise control of FSQ in the present scheme, the corner gates should be designed to create a sharper corner potential. Furthermore, the dephasing should be reduced, e.g., by soft separation of the edges with an extra gate.

## V. CONCLUDING REMARK

We have studied the unitary operation of FSQs in QHECs with electric voltages on metallic gates. This operation utilized the maximal entanglement between spin and edge channel orbitals. The spin rotation in the azimuth angle with voltage and with a magnetic field was systematically studied. A characteristic feature for spin appeared in the rotation in the zenith angle, for which another type of SOI at a corner of the edge channel was introduced and controlled with the gate voltage. With the combination of these two techniques, all-electrical control of electron spin at spin-resolved quantum Hall edge states was achieved.

## ACKNOWLEDGMENTS

We thank S. Sugumaran and L. Beliaev for their collaboration in the initial stage of the present work. This work was partly supported by Grants-in-Aid for Scientific Research on Innovative Areas, “Nano Spin Conversion Science” (Grant No. JP26103003), and by Japan Society for the Promotion of Science KAKENHI Grant No. JP19H00652.

[1] D. Loss and D. P. DiVincenzo, Quantum computation with quantum dots, *Phys. Rev. A* **57**, 120 (1998).

[2] G. Yang, C.-H. Hsu, P. Stano, J. Klinovaja, and D. Loss, Long-distance entanglement of spin qubits via

- quantum Hall edge states, *Phys. Rev. B* **93**, 075301 (2016).
- [3] T. Fujita, T. A. Baart, C. Reichl, W. Wegscheider, and L. M. K. Vandersypen, Coherent shuttle of electron-spin states, *npj Quantum Inf.* **3**, 22 (2017).
- [4] M. Yamamoto, S. Takada, C. Bäuerle, K. Watanabe, A. D. Wieck, and S. Tarucha, Electrical control of a solid-state flying qubit, *Nat. Nanotechnol.* **7**, 247 (2012).
- [5] P. Földi, B. Molnár, M. G. Benedict, and F. M. Peeters, Spintronic single-qubit gate based on a quantum ring with spin-orbit interaction, *Phys. Rev. B* **71**, 033309 (2005).
- [6] S. Gong and Z. Yang, Flying spin-qubit gates implemented through Dresselhaus and Rashba spin-orbit couplings, *Phys. Lett. A* **367**, 369 (2007).
- [7] S. Nadj-Perge, S. M. Frolov, E. P. A. M. Bakkers, and L. P. Kouwenhoven, Spin-orbit qubit in a semiconductor nanowire, *Nature (London)* **468**, 1084 (2010).
- [8] R. Winkler, *Spin-Orbit Coupling Effects in Two-Dimensional Electron and Hole Systems*, Springer Tracts in Modern Physics (Springer, Berlin, 2003).
- [9] M. Büttiker, Time-dependent transport in mesoscopic structures, *J. Low Temp. Phys.* **118**, 519 (2000).
- [10] D. Frustaglia, M. Hentschel, and K. Richter, Quantum Transport in Nonuniform Magnetic Fields: Aharonov-Bohm Ring as a Spin Switch, *Phys. Rev. Lett.* **87**, 256602 (2001).
- [11] E. Schrödinger, Discussion of probability relations between separated systems, *Math. Proc. Cambridge Philos. Soc.* **31**, 555 (1935).
- [12] T. Durt, Quantum entanglement, interaction, and the classical limit, *Z. Naturforsch. A* **59**, 425 (2004).
- [13] A. Einstein, B. Podolsky, and N. Rosen, Can quantum-mechanical description of physical reality be considered complete?, *Phys. Rev.* **47**, 777 (1935).
- [14] W. Gerlach and O. Stern, Der experimentelle nachweis der richtungsquantelung im magnetfeld, *Z. Phys.* **9**, 349 (1922).
- [15] Y. Iwasaki, Y. Hashimoto, T. Nakamura, and S. Katsumoto, Conductance fluctuations in InAs quantum wells possibly driven by Zitterbewegung, *Sci. Rep.* **7**, 7909 (2017).
- [16] V. Giovannetti, F. Taddei, D. Frustaglia, and R. Fazio, Multi-channel architecture for electronic quantum Hall interferometry, *Phys. Rev. B* **77**, 155320 (2008).
- [17] T. Machida, H. Hirai, S. Komiyama, and Y. Shiraki, Phase coherence of edge states over macroscopic length scales, *Phys. B: Condens. Matter* **249-251**, 128 (1998).
- [18] P. Roulleau, F. Portier, P. Roche, A. Cavanna, G. Faini, U. Gennser, and D. Mailly, Direct Measurement of the Coherence Length of Edge States in the Integer Quantum Hall Regime, *Phys. Rev. Lett.* **100**, 126802 (2008).
- [19] R. J. Nicholas, R. J. Haug, K. v. Klitzing, and G. Weimann, Exchange enhancement of the spin splitting in a GaAs-Ga<sub>x</sub>Al<sub>1-x</sub>As heterojunction, *Phys. Rev. B* **37**, 1294 (1988).
- [20] G. F. Giuliani and J. J. Quinn, Spin-polarization instability in a tilted magnetic field of a two-dimensional electron gas with filled Landau levels, *Phys. Rev. B* **31**, 6228 (1985).
- [21] V. Piazza, V. Pellegrini, F. Beltram, W. Wegscheider, T. Jungwirth, and A. H. MacDonald, First-order phase transitions in a quantum Hall ferromagnet, *Nature (London)* **402**, 638 (1999).
- [22] T. Nakajima, K.-t. Lin, and S. Komiyama, Gate-control of spin precession in quantum Hall edge states, [arXiv:1207.7243](https://arxiv.org/abs/1207.7243).
- [23] T. Nakajima, K. T. Lin, and S. Komiyama, Electrical control of flying spin precession in chiral 1D edge states, in *The Physics of Semiconductors: Proceedings of the 31st International Conference on the Physics of Semiconductors (ICPS) 2012*, edited by T. Ihn, C. Rössler, and A. Kozikov, AIP Conf. Proc. Vol. 1566 (AIP, Melville, NY, 2013), p. 301.
- [24] E. V. Deviatov, S. V. Egorov, G. Biasiol, and L. Sorba, Quantum Hall Mach-Zehnder interferometer at fractional filling factors, *Europhys. Lett.* **100**, 67009 (2012).
- [25] E. V. Deviatov and A. Lorke, Experimental realization of a Fabry-Perot-type interferometer by copropagating edge states in the quantum Hall regime, *Phys. Rev. B* **77**, 161302(R) (2008).
- [26] E. V. Deviatov, A. Ganczarczyk, A. Lorke, G. Biasiol, and L. Sorba, Quantum Hall Mach-Zehnder interferometer far beyond equilibrium, *Phys. Rev. B* **84**, 235313 (2011).
- [27] B. Karmakar, D. Venturelli, L. Chirolli, F. Taddei, V. Giovannetti, R. Fazio, S. Roddaro, G. Biasiol, L. Sorba, V. Pellegrini, and F. Beltram, Controlled Coupling of Spin-Resolved Quantum Hall Edge States, *Phys. Rev. Lett.* **107**, 236804 (2011).
- [28] B. Karmakar, D. Venturelli, L. Chirolli, V. Giovannetti, R. Fazio, S. Roddaro, L. N. Pfeiffer, K. W. West, F. Taddei, and V. Pellegrini, Nanoscale Mach-Zehnder interferometer with spin-resolved quantum Hall edge states, *Phys. Rev. B* **92**, 195303 (2015).
- [29] M. Hashisaka, N. Hiyama, T. Akiho, K. Muraki, and T. Fujisawa, Waveform measurement of charge- and spin-density wavepackets in a chiral Tomonaga-Luttinger liquid, *Nat. Phys.* **13**, 559 (2017).
- [30] M. Hashisaka and T. Fujisawa, Tomonaga-Luttinger-liquid nature of edge excitations in integer quantum Hall edge channels, *Rev. Phys.* **3**, 32 (2018).
- [31] D. Yoshioka, *The Quantum Hall Effect*, Springer Series in Solid-State Sciences Vol. 133 (Springer, Berlin, 2002).
- [32] A. Aharony, O. Entin-Wohlman, B. I. Halperin, and Y. Imry, Phase measurement in the mesoscopic Aharonov-Bohm interferometer, *Phys. Rev. B* **66**, 115311 (2002).
- [33] See Supplemental Material at <http://link.aps.org/supplemental/10.1103/PhysRevB.102.235302> for more information on the depth of two-dimensional electrons calculated with the Poisson-Schrödinger approximation, quantum Hall characteristics, conductance versus the voltages on gate L and the external magnetic fields, intuitive description of the minimum point of  $\Delta y$  against  $V_C$ , estimation of  $\Delta y$  from  $\Delta B$ , electrostatic potential around a gate corner, and effects of inner edge channels in the  $\nu = 4$  quantum Hall state.
- [34] I. Strzalkowski, S. Joshi, and C. R. Crowell, Dielectric constant and its temperature dependence for GaAs, CdTe, and ZnSe, *Appl. Phys. Lett.* **28**, 350 (1976).
- [35] D. B. Chklovskii, B. I. Shklovskii, and L. I. Glazman, Electrostatics of edge channels, *Phys. Rev. B* **46**, 4026 (1992).
- [36] I. A. Larkin and J. H. Davies, Edge of the two-dimensional electron gas in a gated heterostructure, *Phys. Rev. B* **52**, R5535 (1995).
- [37] K. Oto, S. Takaoka, and K. Murase, Width of compressible strips in quantum Hall regime, *Phys. B: Condens. Matter* **298**, 18 (2001).

- [38] S. Masubuchi, K. Hamaya, and T. Machida, Gate-controlled nuclear magnetic resonance in an AlGaAs/GaAs quantum Hall device, *Appl. Phys. Lett.* **89**, 202111 (2006).
- [39] H. Kamata, T. Ota, K. Muraki, and T. Fujisawa, Voltage-controlled group velocity of edge magnetoplasmon in the quantum Hall regime, *Phys. Rev. B* **81**, 085329 (2010).
- [40] S. Komiyama, H. Hirai, M. Ohsawa, Y. Matsuda, S. Sasa, and T. Fujii, Inter-edge-state scattering and nonlinear effects in a two-dimensional electron gas at high magnetic fields, *Phys. Rev. B* **45**, 11085 (1992).
- [41] K. Y. Chen, C. S. Chu, and A. G. Mal'shukov, Resonant spin dipole induced by an in-plane potential gradient spin-orbit interaction, *Phys. Rev. B* **76**, 153304 (2007).
- [42] J. R. Rubbmark, M. M. Kash, M. G. Littman, and D. Kleppner, Dynamical effects at avoided level crossings: A study of the Landau-Zener effect using Rydberg atoms, *Phys. Rev. A* **23**, 3107 (1981).